ELSEVIER

Powder Technology 116 (2001) 166–177

POWDER TECHNOLOGY

www.elsevier.com/locate/powtec

Experimental validation of granular dynamics simulations of gas-fluidised beds with homogenous in-flow conditions using Positron Emission Particle Tracking

B.P.B. Hoomans [a,1], J.A.M. Kuipers [a,*], M.A. Mohd Salleh [b], M. Stein [b,2], J.P.K. Seville [b]

[a] *Department of Chemical Engineering, University of Twente, P.O. Box 217, 7500 AE Enschede, Netherlands*
[b] *School of Chemical Engineering and Positron Imaging Centre, University of Birmingham, Edgbaston, Birmingham B15 2TT, UK*

Received 3 April 2000; received in revised form 1 August 2000; accepted 18 August 2000

Abstract

A hard-sphere granular dynamics model of a two-dimensional gas-fluidised bed was experimentally validated using Positron Emission Particle Tracking (PEPT). In the model the Newtonian equations of motion are solved for each solid particle while taking into account the particle–particle and particle–wall collisions. The gas phase hydrodynamics is described by the spatially averaged Navier–Stokes equations for two-phase flow. A quasi two-dimensional (i.e. narrow) bed of 0.185-m width and 0.4-m height with homogenous inflow conditions at 1.5 u_{mf} was chosen as a test case. Glass particles ($\rho_p = 2435$ kg/m^3) with diameters ranging from 1.25 to 1.5 mm were used as the bed material. The collision parameters required in the simulation were obtained from separate, independent measurements. In the PEPT experiment, the motion of a single tracer particle in the bed was tracked for 1 h. In the simulation, the motion of 15,000 particles was tracked for 45 s. The simulation data were time-averaged over 45 s for each particle and subsequently ensemble-averaged over all the particles in the simulation. The comparison was made on the basis of averaged velocity maps, "occupancy" plots and speed histograms. The results showed good agreement between experiment and simulation when the measured values for the collision parameters were used. When collisions were assumed to be fully elastic and perfectly smooth the agreement was much worse.

Keywords: Granular dynamics simulations; Gas-fluidised beds; Positron Emission Particle Tracking

1. Introduction

In order to predict the performance of fluidised bed reactors, it is necessary to develop robust and verifiable flow models. This paper concerns the experimental validation of such models. The trend in both experiments and models is that systems can be studied in more and more detail with continuously increasing accuracy. It is not the objective here to present a complete review of available experimental techniques for gas-fluidised beds. A comprehensive review of measuring techniques in fluidised beds was presented by Werther [30] and an extensive overview of existing techniques for the measurement of solids concentration and velocity was presented by Nieuwland et al. [15].

With increasing computer power, Granular Dynamics has become a very useful and versatile research tool to study the dynamics of dense gas-particle flows [6]. In these models, the Newtonian equations of motion are solved for each individual granular particle in the system. The mutual interactions between particles and the interaction between particles and walls are taken into account directly. The discrete particle approach was pioneered by Tsuji et al. [26] who used a "soft-sphere" model to describe the interaction between the particles. A three-dimensional version of this model was later presented by Kawaguchi et al. [12], whereas Mikami et al. [13] extended the (2D) model in order to include cohesive forces between the particles. Hoomans et al. [5] presented a "hard-sphere" approach

* Corresponding author. Tel.: +31-53-489-3039; fax: +31-53-489-4774.
E-mail addresses: Bob.Hoomans@dsm-group.com (B.P.B. Hoomans), J.A.M.Kuipers@ct.utwente.nl (J.A.M. Kuipers).
[1] Present address: DSM Research, P.O. Box 18, 6160 MD Geleen, The Netherlands.
[2] Present address: Unilever Research Colworth, Bedford MK44 1LQ, UK.

0032-5910/01/$ - see front matter
PII: S0032-5910(00)00391-0

where collisions are assumed to be binary and instantaneous. Xu and Yu [32] developed a hybrid technique combining elements of both soft-sphere and hard-sphere techniques. In the studies on discrete particle simulation of gas-fluidised beds, previously reported in the literature, experimental validation has received little attention. This was partly due to the fact that proper experimental techniques were not widely available.

Experimental validation can be performed by direct observation of transient phenomena in a transparent system by using a video camera. This is a very basic technique that nonetheless can provide useful information on for instance the formation of a single bubble at an orifice or the dynamics of segregation. In the latter case, it is required that the segregating species can be visually identified. However, the direct observation technique is limited to optically transparent systems in contrast to, for example, X-ray techniques [33]. Furthermore, the information that is obtained using direct observation covers macroscopic behaviour: important quantities such as local solids volume fraction and local solids velocities cannot be obtained using this technique.

Non-invasive particle tracking techniques are ideally suited to the validation of discrete particle models since direct comparison between measured data and simulation results is possible. Lin et al. [10] presented a "proximity" technique where a radioactive tracer particle of scandium-46 (Sc-46) was used. Twelve scintillation detectors were positioned around the fluidised bed to enable determination of the location of the particle. More recently, Larachi et al. [9] applied the tracking technique using Sc-46 tracers to gas–liquid–solid flows and Mostoufi and Chaouki [14] applied the technique to liquid-fluidised beds.

In this work a cooperation between the University of Twente and the University of Birmingham was initiated in order to use the Positron Emission Particle Tracking (PEPT) technique developed at Birmingham to validate the granular dynamics model of a gas-fluidised bed developed at Twente. PEPT has been developed at Birmingham since 1987 [16] and has been successfully applied to a large number of systems for solids processing including mixers and gas-fluidised beds [19]. A comprehensive introduction to PEPT can be found in Stein et al. [20]. Recently a PEPT system was also developed by Stellema et al. [22]. PEPT differs from other tracking techniques in the sense that it uses positron-emitting radioisotopes that have the unique feature that their decay leads to simultaneous emission of a pair of back-to-back γ-rays. In Section 2 a more elaborate discussion of the PEPT technique will be presented.

2. Model

In the hard-sphere model used in this work the particles are assumed to interact through binary, instantaneous collisions where contact occurs at a point. The particles are perfect, homogeneous spheres and the interaction forces are impulsive. Between collisions the particles are in free flight. First the collision model will be presented and then the computational strategy and some optimisation techniques will be described. The collision model will be presented in vector notation. For the 2-D version used in this work, the *z*-components of the position and velocity vectors are zero and only rotation about the *z*-axis is considered. A more detailed description can be found in Hoomans [6].

2.1. Collision model

In the collision model it is assumed that the interaction forces are impulsive and therefore all other finite forces are negligible during collision. The original collision model [5] was mapped after the model presented by Wang and Mason [29]. However, in this work we will mainly adopt the notation used by Foerster et al. [3] since that is more widely accepted (see for example Refs. [11, 27]). The coordinate systems used in our model are defined in Fig. 1.

Consider the two colliding spheres a and b in Fig. 1 with position vectors $\boldsymbol{r}_a$ and $\boldsymbol{r}_b$. The normal unit vector can now be defined:

$$\boldsymbol{n} = \frac{\boldsymbol{r}_a - \boldsymbol{r}_b}{|\boldsymbol{r}_a - \boldsymbol{r}_b|}. \tag{1}$$

Hence, the normal unit vector points in the direction from the centre of particle *b* to the centre of particle *a*. The point of origin is the contact point.

Prior to collision, the spheres with radii R_a and R_b and masses m_a and m_b have translation velocity vectors $\boldsymbol{v}_a$ and $\boldsymbol{v}_b$ and rotational velocity vectors $\boldsymbol{\omega}_a$ and $\boldsymbol{\omega}_b$ (clockwise rotation is negative by definition). Velocities prior-to-collision are indicated by the subscript 0.

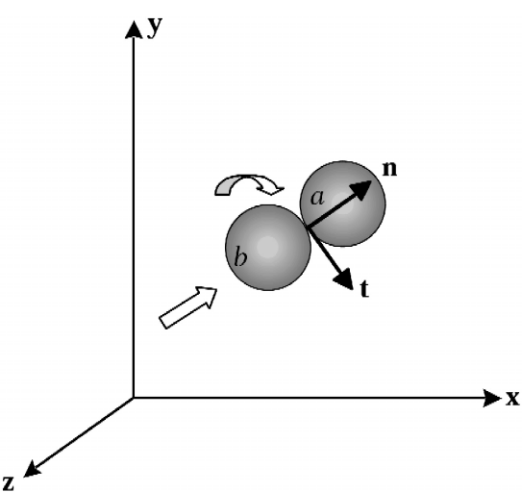

Fig. 1. Definition of the coordinate systems.

For a binary collision of these spheres the following equations can be derived by applying Newton's second and third laws:

$$m_a(\boldsymbol{v}_a - \boldsymbol{v}_{a,0}) = \boldsymbol{J}, \tag{2}$$

$$m_b(\boldsymbol{v}_b - \boldsymbol{v}_{b,0}) = -\boldsymbol{J}, \tag{3}$$

$$I_a(\boldsymbol{\omega}_a - \boldsymbol{\omega}_{a,0}) = -(R_a\boldsymbol{n}) \times \boldsymbol{J}, \tag{4}$$

$$I_b(\boldsymbol{\omega}_b - \boldsymbol{\omega}_{b,0}) = -R_b\boldsymbol{n} \times (-\boldsymbol{J}), \tag{5}$$

$$m_a(\boldsymbol{v}_a - \boldsymbol{v}_{a,0}) = -m_b(\boldsymbol{v}_b - \boldsymbol{v}_{b,0}) = \boldsymbol{J}, \tag{6}$$

$$\frac{I_a}{R_a}(\boldsymbol{\omega}_a - \boldsymbol{\omega}_{a,0}) = \frac{I_b}{R_b}(\boldsymbol{\omega}_b - \boldsymbol{\omega}_{b,0}) = -\boldsymbol{n} \times \boldsymbol{J}, \tag{7}$$

$$I = \frac{2}{5}mR^2. \tag{8}$$

The impulse vector $\boldsymbol{J}$ is defined as follows:

$$\boldsymbol{J} = \int_{t=0}^{t=t_c} \boldsymbol{F}_{ab}\,\mathrm{d}t, \tag{9}$$

where t_c stands for the contact time (i.e. the duration of the contact).

From Eqs. (6) and (7) it is clear that the post-collision velocities of both particles can be calculated when the impulse vector $\boldsymbol{J}$ is known. If the force $\boldsymbol{F}_{ab}$ in Eq. (9) were known as a function of all the parameters involved, the impulse $\boldsymbol{J}$ could be calculated directly. Thornton [25] demonstrated that based on a simplified theoretical model for the normal interaction between elastic-perfectly plastic spheres an analytical solution could be obtained for the rebound velocity. Walton [28] used two types of finite element codes (DYNA2D and NIKE2D) to simulate the collision process in detail on a more microscopic level. The only input parameters necessary in these calculations are material properties although assumptions have to be made about the deformation behaviour (elastic/plastic) of the material. In simulations of gas-fluidised beds a large number of collisions (typically 10^6–10^9) have to be processed and therefore the actual physics of a binary collision has to be simplified to some extent and constitutive relations have to be introduced.

Before these constitutive relations are introduced, the relative velocity at the contact point ($\boldsymbol{v}_{ab}$) has to be defined:

$$\boldsymbol{v}_{ab} \equiv (\boldsymbol{v}_{a,c} - \boldsymbol{v}_{b,c}). \tag{10}$$

$$\boldsymbol{v}_{ab} = (\boldsymbol{v}_a - \boldsymbol{\omega}_a \times R_a\boldsymbol{n}) - (\boldsymbol{v}_b + \boldsymbol{\omega}_b \times R_b\boldsymbol{n}). \tag{11}$$

$$\boldsymbol{v}_{ab} = (\boldsymbol{v}_a - \boldsymbol{v}_b) - (R_a\boldsymbol{\omega}_a + R_b\boldsymbol{\omega}_b) \times \boldsymbol{n}. \tag{12}$$

From this relative velocity, the tangential unit vector can be obtained since the normal unit vector is already defined in Eq. (1):

$$\boldsymbol{t} = \frac{\boldsymbol{v}_{ab,0} - \boldsymbol{n}(\boldsymbol{v}_{ab,0} \cdot \boldsymbol{n})}{|\boldsymbol{v}_{ab,0} - \boldsymbol{n}(\boldsymbol{v}_{ab,0} \cdot \boldsymbol{n})|}. \tag{13}$$

Eqs. (6) and (7) can now be rearranged using $(\boldsymbol{n} \times \boldsymbol{J}) \times \boldsymbol{n} = \boldsymbol{J} - \boldsymbol{n}(\boldsymbol{J} \cdot \boldsymbol{n})$ and Eq. (12) to obtain:

$$\boldsymbol{v}_{ab} - \boldsymbol{v}_{ab,0} = B_1\boldsymbol{J} - (B_1 - B_2)\boldsymbol{n}(\boldsymbol{J} \cdot \boldsymbol{n}), \tag{14}$$

where

$$B_1 = \frac{7}{2}\left(\frac{1}{m_a} + \frac{1}{m_b}\right), \tag{15}$$

and

$$B_2 = \frac{1}{m_a} + \frac{1}{m_b}. \tag{16}$$

At this point constitutive relations are required to close the set of equations. Through these constitutive relations, three parameters enter the model. The first parameter is the coefficient of (normal) restitution, ($0 \le e \le 1$):

$$\boldsymbol{v}_{ab} \cdot \boldsymbol{n} = -e(\boldsymbol{v}_{ab,0} \cdot \boldsymbol{n}). \tag{17}$$

For non-spherical particles, this definition can lead to energy inconsistencies [23], however, for spherical particles this definition holds. The second parameter is the coefficient of (dynamic) friction, ($\mu \ge 0$):

$$|\boldsymbol{n} \times \boldsymbol{J}| = -\mu(\boldsymbol{n} \cdot \boldsymbol{J}). \tag{18}$$

The third parameter is the coefficient of tangential restitution, ($0 \le \beta_0 \le 1$):

$$\boldsymbol{n} \times \boldsymbol{v}_{ab} = -\beta_0(\boldsymbol{n} \times \boldsymbol{v}_{ab,0}). \tag{19}$$

Notice that this relation does not affect the components parallel to $\boldsymbol{n}$ and that the components orthogonal to $\boldsymbol{n}$ are related by a factor—β_0. Although it is accepted that these coefficients depend on particle size and impact velocity, this is not taken into account in this model. The only exception is made for the coefficient of normal restitution where collisions occurring at a normal impact velocity less than a threshold value (typically 10^{-4} m/s) are assumed to be perfectly elastic ($e = 1.0$). The coefficient of tangential restitution and the threshold value for the normal coefficient of restitution were not included in the model used by Hoomans et al. [5]. The threshold value was mainly introduced for computational convenience. It does not have a significant effect on the simulation results.

Combining Eqs. (14) and (17) yields the following expression for the normal component of the impulse vector:

$$J_n = -(1 + e)\frac{\boldsymbol{v}_{ab,0} \cdot \boldsymbol{n}}{B_2}. \tag{20}$$

For the tangential component, two types of collisions can be distinguished that are called *sticking* and *sliding*. If the tangential component of the relative velocity is sufficiently high in comparison to the coefficients of friction and tangential restitution that gross sliding occurs throughout the whole duration of the contact, the collision is of the *sliding* type. The non-sliding collisions are of the *sticking* type. When β_0 is equal to zero the tangential component of the relative velocity becomes zero during a *sticking*

collision. When β_0 is greater than zero in such a collision, reversal of the tangential component of the relative velocity will occur. The criterion to determine the type of collision is as follows:

$$\mu < \frac{(1+\beta_0)\boldsymbol{v}_{ab,0}\cdot\boldsymbol{t}}{J_n B_1} \qquad \text{sliding,} \tag{21}$$

$$\mu \geq \frac{(1+\beta_0)\boldsymbol{v}_{ab,0}\cdot\boldsymbol{t}}{J_n B_1} \qquad \text{sticking.} \tag{22}$$

For collisions of the sticking type, the tangential impulse is given by:

$$J_t = -(1+\beta_0)\frac{|\boldsymbol{n}\times\boldsymbol{v}_{ab,0}|}{B_1} = -(1+\beta_0)\frac{\boldsymbol{v}_{ab,0}\cdot\boldsymbol{t}}{B_1}. \tag{23}$$

For collisions of the sliding type, the tangential impulse is given by:

$$J_t = -\mu J_n. \tag{24}$$

The total impulse vector is then simply obtained by addition:

$$\boldsymbol{J} = J_n\boldsymbol{n} + J_t\boldsymbol{t}. \tag{25}$$

The post-collision velocities can now be calculated from Eqs. (6) and (7).

In particle–wall collisions the mass of particle b (i.e. the wall) is infinitely large, which makes all terms $1/m_b$ equal to zero. It is possible to implement a moving/rotating wall through the velocity vectors $\boldsymbol{v}_b$ and $\boldsymbol{\omega}_b$ but in the simulations performed for this work these velocities are all set equal to zero.

2.2. Granular dynamics

In the hard-sphere approach a sequence of binary collisions is processed. This implies that a collision list is compiled in which for each particle a collision partner and a corresponding collision time is stored. A constant time step is used to take the external forces into account, and *within* this time step, the prevailing collisions are processed sequentially. Hence, the force balance is not updated in between each collision but this is allowed since the macroscopic behaviour (i.e. bubble formation) observed in the simulations proved rather insensitive to the magnitude of the time step [6]. In order to reduce the required CPU time, neighbour lists are used. For each particle, a list of neighbouring particles is stored and a check for possible collisions is performed only for the particles in this list. A detailed description of this technique was presented by Hoomans et al. [5].

2.3. External forces

The incorporation of external forces differs somewhat from the approach followed by Hoomans et al. [5]. In this work the external forces are in accordance with those implemented in the two-fluid model presented by Kuipers et al. [7] where, of course, the forces now act on a single particle:

$$m_p\frac{d\boldsymbol{v}_p}{dt} = m_p g + \frac{V_p\beta}{(1-\varepsilon)}(\boldsymbol{u}-\boldsymbol{v}_p) - V_p\nabla p, \tag{26}$$

where m_p represents the mass of a particle, $\boldsymbol{v}_p$ its velocity, $\boldsymbol{u}$ the local gas velocity and V_p the volume of a particle. In Eq. (26) the first term is due to gravity and the third term is the force due to the pressure gradient. The second term is due to the drag force where β represents an inter-phase momentum exchange coefficient as it usually appears in two-fluid models. For low void fractions ($\varepsilon < 0.80$) β is obtained from the well-known Ergun equation:

$$\beta = 150\frac{(1-\varepsilon)^2}{\varepsilon}\frac{\mu_g}{D_p^2} + 1.75(1-\varepsilon)\frac{\rho_g}{D_p}|\boldsymbol{u}-\boldsymbol{v}_p|, \tag{27}$$

where D_p represents the particle diameter, μ_g the viscosity of the gas and ρ_g the density of the gas. For high void fractions ($\varepsilon \geq 0.80$) the following expression for the inter-phase momentum transfer coefficient has been used, which is basically the correlation presented by Wen and Yu [31] who extended the work of Richardson and Zaki [18]:

$$\beta = \frac{3}{4}C_d\frac{\varepsilon(1-\varepsilon)}{D_p}\rho_g|\boldsymbol{u}-\boldsymbol{v}_p|\varepsilon^{-2.65}. \tag{28}$$

The drag coefficient C_d is a function of the particle Reynolds number and given by:

$$C_d = \begin{cases} \dfrac{24}{Re_p}\left(1+0.15Re_p^{0.687}\right) & Re_p < 1000 \\ 0.44 & Re_p \geq 1000 \end{cases}, \tag{29}$$

where the particle Reynolds number (Re_p) in this case is defined as follows:

$$Re_p = \frac{\varepsilon\rho_g|\boldsymbol{u}-\boldsymbol{v}_p|D_p}{\mu_g}. \tag{30}$$

For the integration of Eq. (26), a simple explicit first order scheme was used to update the velocities and positions of the particles.

2.4. Gas phase hydrodynamics

The calculation of the gas phase hydrodynamics mainly follows the lines presented by Kuipers et al. [7]. It is based on the numerical solution of the following set of partial differential equations that can be seen as a generalised form of the Navier–Stokes equations for a gas interacting with a solid phase as originally derived by Anderson and Jackson [1].

Continuity equation gas phase:

$$\frac{\partial(\varepsilon\rho_g)}{\partial t} + (\nabla\cdot\varepsilon\rho_g\boldsymbol{u}) = 0. \quad (31)$$

Momentum equation gas phase:

$$\frac{\partial(\varepsilon\rho_g\boldsymbol{u})}{\partial t} + (\nabla\cdot\varepsilon\rho_g\boldsymbol{u}\boldsymbol{u}) = -\varepsilon\nabla p - \boldsymbol{S}_p - (\nabla\cdot\varepsilon\tau_g) + \varepsilon\rho_g\boldsymbol{g}. \quad (32)$$

In this work transient, two-dimensional, isothermal (T = 293 K) flow of air at atmospheric conditions is considered. The constitutive equations (ideal gas law, Newtonian rheology) are the same as presented previously by Hoomans et al. [5].

2.5. Two-way coupling

Two-way coupling between the motion of the particles and the motion of the gas phase is established through the calculation of the void fraction (ε) and the source term (S_p) in the momentum conservation equation of the gas

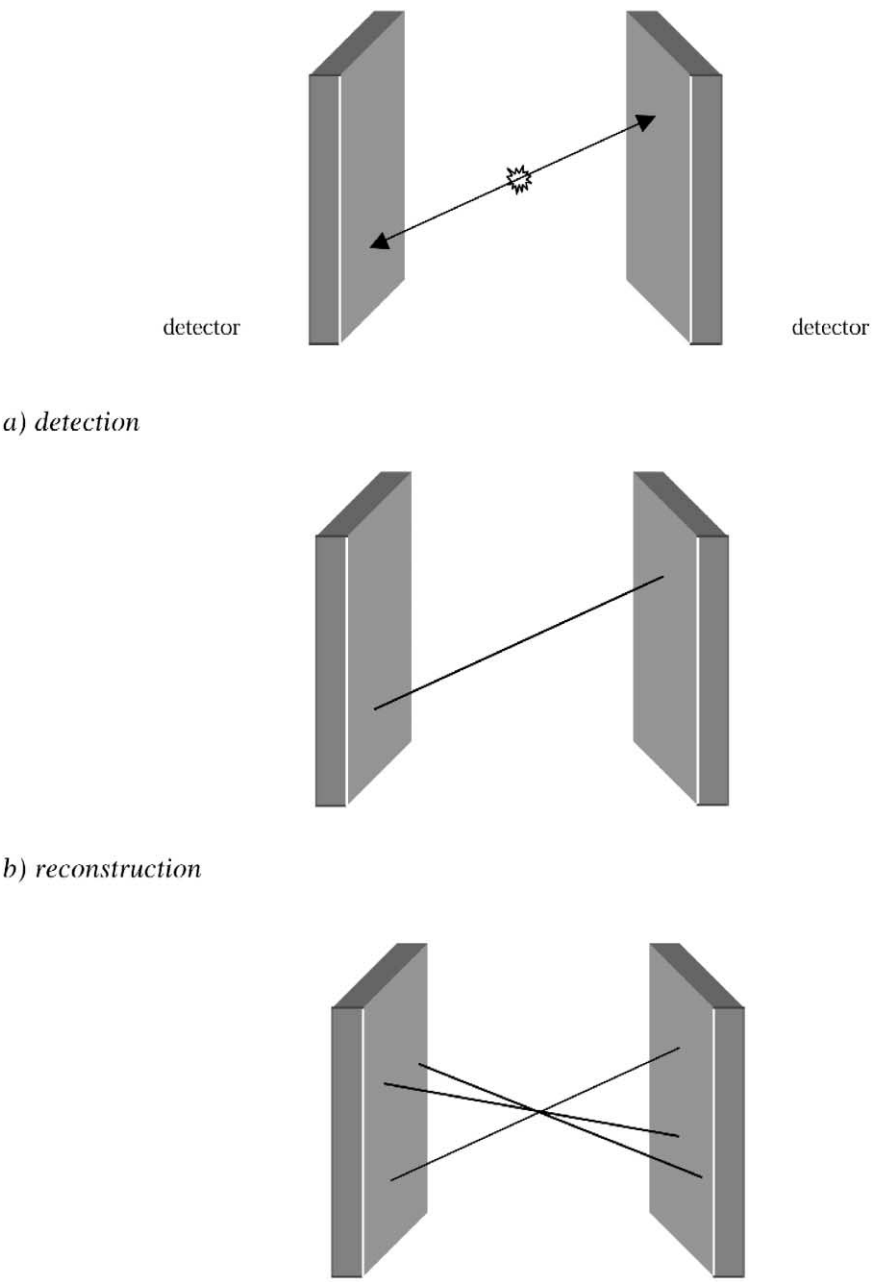

Fig. 2. The principle of the PEPT technique.

phase. The void fraction is calculated based on a two-dimensional analysis that is inconsistent with the applied empiricism in the calculation of the drag force exerted on a particle. To correct for this inconsistency the void fraction calculated on the basis of area (ε_{2D}) is transformed into a three-dimensional void fraction (ε_{3D}) using the following equation:

$$\varepsilon_{3D} = 1 - \frac{2}{\sqrt{\pi\sqrt{3}}}(1-\varepsilon_{2D})^{3/2}. \quad (33)$$

This equation has been derived on the basis of a comparison between a two-dimensional hexagonal lattice and a three-dimensional FCC unit cube assuming equal inter-particle distances. It ensures that the closest packing in the 2-D hexagonal lattice is transformed into the closest packing in the 3-D FCC case. The same transformation function was applied by Drake [2].

An important modification with respect to the model presented by Hoomans et al. [5] deals with the implementation of the source term (S_p) in the gas phase momentum conservation Eq. (32). In the present model, the reaction force to the drag force exerted on a particle per unit of volume is fed back to the gas phase through the source term S_p that has the dimension of force per unit of volume N/m^3:

$$S_p = -\frac{1}{V}\int \sum_{a=0}^{Npart} \frac{V_p \beta}{(1-\varepsilon)}(\boldsymbol{u}-\boldsymbol{v}_a)\,\delta(\boldsymbol{r}-\boldsymbol{r}_a)\mathrm{d}V. \quad (34)$$

The δ-function ensures that the reaction force acts as at a point at the position of the particle in the system. In the numerical implementation, this force-per-volume term is distributed to the four nearest grid nodes using an area-weighted averaging technique described earlier by Hoomans et al. [5]. A mixed explicit–implicit numerical treatment was applied similar to the one used by Kuipers et al. [8] to solve the gas phase conservation equations.

Since the source term S_p has the dimension of force per unit volume the force exerted on the particles has to be divided by the volume of a grid cell. In a 3-D model, this is straightforward since the third dimension is determined by the depth of the bed. In the 2-D model applied in this work, a virtual third dimension has to be introduced. This virtual third dimension is estimated based on the same calculation as the conversion from ε_{2D} to ε_{3D}. In the 2-D simulations, the volume of a computational cell was chosen to be:

$$V_{cell} = 2DXDY3^{-0.75}D_p, \quad (35)$$

in which the third dimension is slightly less than the particle diameter. Note that this volume depends on the particle size, and hence, is not a constant in simulations where a particle size distribution is taken into account.

3. Positron Emission Particle Tracking

Positron Emission Particle Tracking (PEPT) is a technique that allows non-invasive observation of the motion of a single radioactive tracer particle. The PEPT technique is schematically represented in Fig. 2. In the experiment reported here, a glass particle, taken from the sample of particles used in the fluidisation experiment, was activated by direct irradiation in a cyclotron beam. The glass particle was irradiated with the ^{3}He beam from a cyclotron to produce the positron emitter ^{18}F from reactions involving the oxygen on the glass. The decay of the ^{18}F isotope features the conversion of a proton to a neutron with the emission of a positron, the anti-particle of the electron. The positron then annihilates with an electron to produce a pair of back-to-back γ-rays. The γ-rays are detected by the positron camera, which consists of two position-sensitive γ-ray detectors, each with an active area of 0.3 by 0.6 m. By using a reconstruction algorithm the position of the particle can be obtained as the intersection point of successive annihilation vectors [16]. The algorithm employs an iterative scheme to discard corrupt annihilation vectors that can be caused by γ-ray scattering or random coincidences. When the tracer particle is stationary the more annihilation vectors are used the more accurately the particle position can be determined. However, when the particle is moving the set of annihilation vectors should be large enough to locate the particle accurately but not so large that it has moved significantly during the time period over which the set was measured.

The instantaneous particle velocity vector can be obtained from the difference between successive particle locations. The data consist of a list of tracer coordinates (r_{xi}, r_{yi}, r_{zi}) each with its associated time t_i. In practice, a weighted rolling average of 6 differences between locations i and $i+5$ is used, and is in general accurate to within 10% [17].

4. Comparison between PEPT data and simulation

The PEPT experiment as performed in this work yields the trajectory of a single particle during 1 h. This time

Table 1
Parameter settings for the PEPT simulation

Particles		Bed	
Shape	spherical	Width	0.185 m.
density, ρ_p	2418 kg/m^3	Height	0.40 m
particle diameter, D_p	1.25–1.50 mm	Number x-cells, NX	37
$e = e_w$	0.97	Number y-cells, NY	80
$\mu = \mu_w$	0.10	cell width, DX	5 mm
$\beta_0 = \beta_{0,w}$	0.33	cell height, DY	5 mm
N_p	15,000	time step, DT	10^{-4} s

scale cannot be reached by means of simulation on modern day computers. Instead, the motion of 15,000 particles is tracked during a shorter period of time (45 s). In fact considerably more data is generated in the simulation since 15,000 times 45 s is a far larger number than 1 times 3600 s. And since the 15,000 simulated particles cover the whole of the fluidised system, the simulation data does not suffer from poorly sampled regions.

It is assumed that it is justified to compare the simulation results with the time-averaged experimental data by first time-averaging the simulation data for each of the 15,000 particles and subsequently taking an ensemble average over all the 15,000 particles. In doing this, there is a risk that rare events, which occur over a time scale close to or greater than the duration of a simulation, are poorly sampled. On the other hand, the chance that such a rare event is experienced by the tracer particle in the experiment is rather low as well.

The actual comparison is made on the basis of "occupancy" plots, velocity maps and speed histograms which

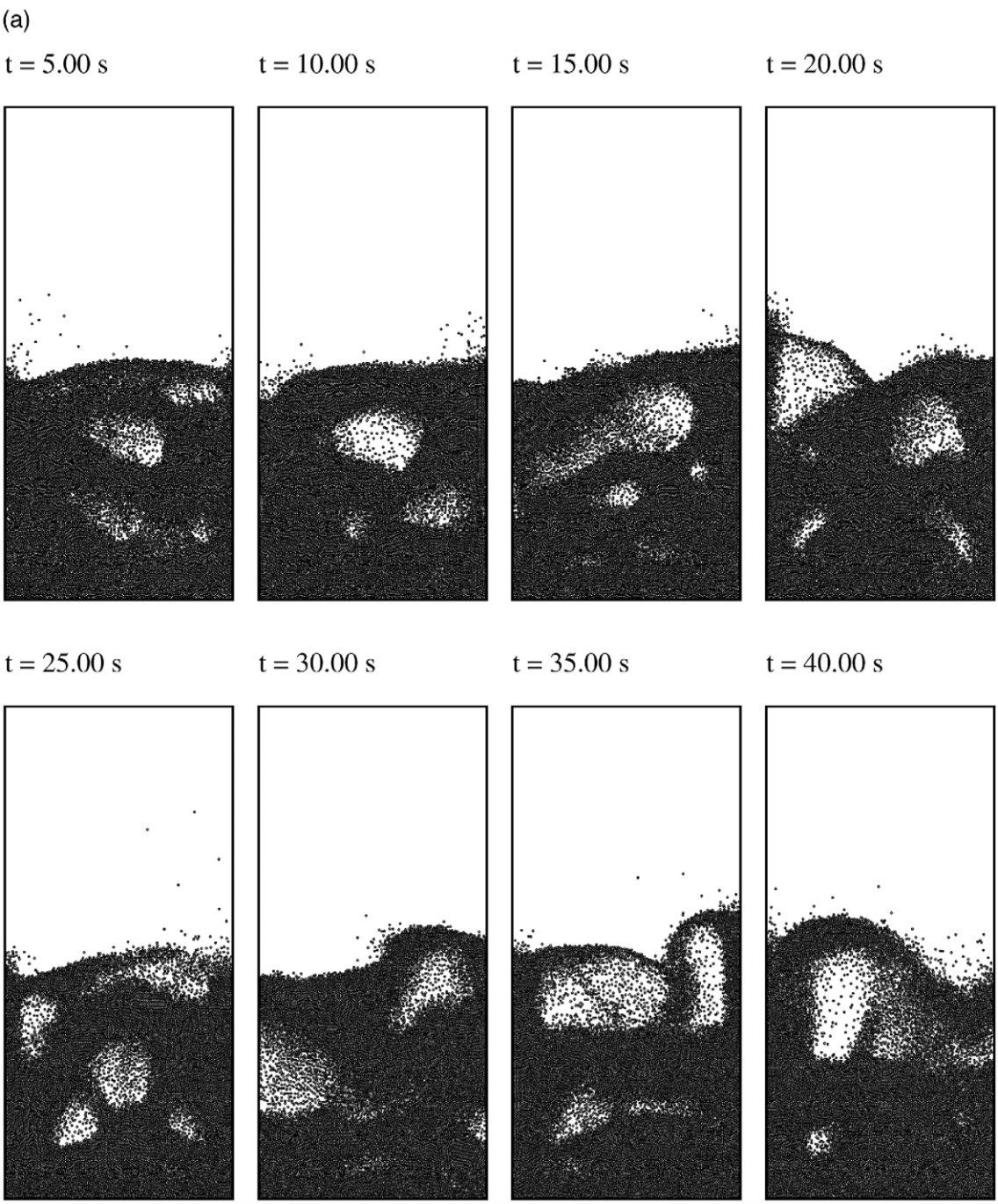

Fig. 3. (a) Snapshots of particle configurations of the simulation at a 5 second interval, (b) snapshots of the PEPT experiment.

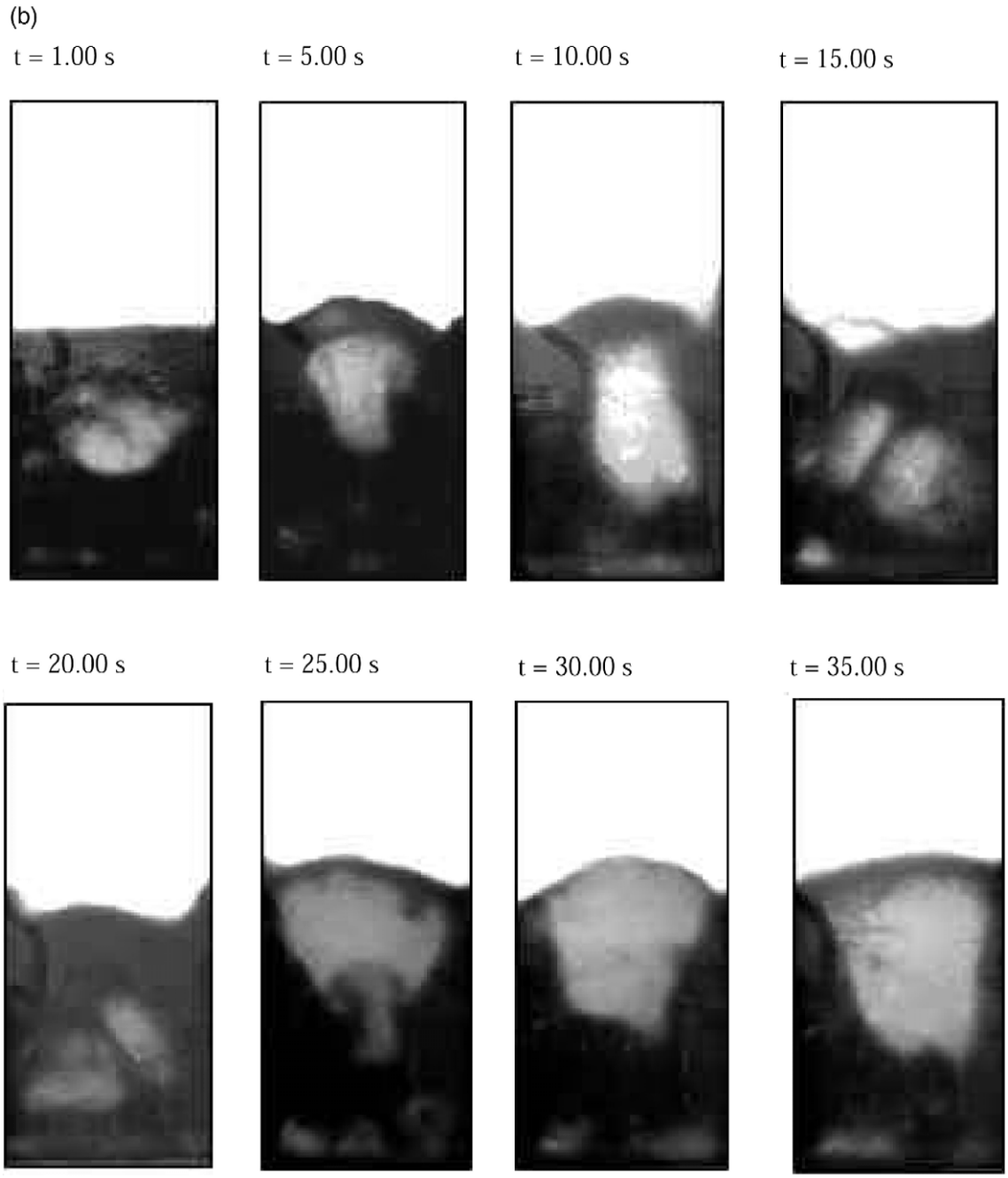

Fig. 3 (*continued*).

are standard outputs of the PEPT software [24] developed by the University of Birmingham. To obtain an occupancy plot from the PEPT data the system is first divided into cells (in this case, 10 mm width/height). Occupancy is defined here as the fraction of the run time, which the tracer particle spends in each volume element. This fraction is displayed using a colour code that is explained in the legend accompanying the plot. Note that occupancy does not distinguish between a few long "visits" and many shorter ones. For the simulations, a similar procedure was followed after all the individual particle trajectories were added together. The velocity vectors presented in the velocity maps are cell-based time-averages. Finally, the PEPT data were compared with the results of the simulation using speed histograms. For the PEPT experiment the speed of the tracer particle was calculated on the basis of the three velocity components (x, y, z) at each instant. The histogram shows the speed distribution based on the data set covering the entire duration of the experiment of 1 h. The speed histograms obtained from the simulation results are based on the two velocity components (x, y) taken into account in the simulations.

5. Results

As a test system for the experimental validation, a gas-fluidised bed (0.185 m width, 20 mm depth) with homogeneous in-flow conditions ($u_g = 1.5\ u_{mf}$, $u_{mf} = 0.9$ m/s) was chosen. The vertical walls were of glass and the gas distributor format from sintered bronze. The parameter settings for the simulation are summarised in Table 1. The bed was filled with the glass particles in such a way the static bed height was about 0.17 m. In the simulation, a total number of 15,000 particles was used to match the bed height encountered in the experiment.

The particle–particle collision parameters presented in Table 1 were independently measured by Gorham and Kharaz [4] using the facility at the Open University at Milton Keynes. The particle-wall collision parameters were assumed to be equal to the particle–particle collision parameters. This is justified since earlier simulations showed that the influence of the particle–wall collision parameters were negligible compared to the influence of the particle–particle collision parameters for $0.8 < e \leq 1.0$ [6]. A log-normal particle size distribution about an average diameter of 1.375 mm was taken into account in the simulation. Particle diameters lower than 1.25 mm and greater than 1.50 mm were rejected in order to mimic the effects of sieving and hence match the particle size distribution encountered in the experiment.

An initial simulation was performed first to ensure that the actual simulation would not suffer from any start-up effects. During this initial simulation the system was operated at a homogeneous gas inflow of 1.5 u_{mf} ($u_{mf} = 0.9$ m/s) for 15 s with the parameter settings presented in Table 1. After this initial simulation the actual simulation (duration 45 s) was started and the required data (positions and velocities) were stored at time intervals corresponding to those used in the experiment. Snapshots of the simulation (5-s interval) are presented in Fig. 3a. In Fig. 3b, snapshots are presented that were obtained from the experimental set-up using a photo camera. In this figure, it can be observed that the bed is bubbling quite vigorously, which is even more the case in the experiment than in the simulation. In Fig. 4, an example of the trajectory of one single (randomly chosen) particle in the simulation is presented. This trajectory covers the whole duration of the simulation of 45 s. Although this figure gives some insight into the motion of a particle in a fluidised bed it does not provide a solid basis for a comparison. Therefore, averaging techniques were applied as discussed in the previous section, which yield data that permit a comparison between the PEPT data and the simulation results.

In Fig. 5 the velocity map obtained from the PEPT data is presented together with the velocity maps obtained from two simulations. In the centre, the velocity map of the simulation using the measured values for the collision parameters (Table 1) is presented, and on the right the velocity map of a simulation assuming fully elastic, perfectly smooth collisions ($e = 1$, $\mu = 0$, also referred to as *ideal* collisions). A reference vector indicating the magnitude of the velocity is included. For the simulations a reference vector of magnitude 0.4 m/s is plotted next to the lower right corner of the system. In the velocity map of the PEPT data, a circulation pattern can be observed where particles rise in the centre of the bed and descend near the walls. Two circulation cells can be distinguished which together form a rather symmetric picture indicating that the gas inflow at the distributor plate was indeed homogeneous.

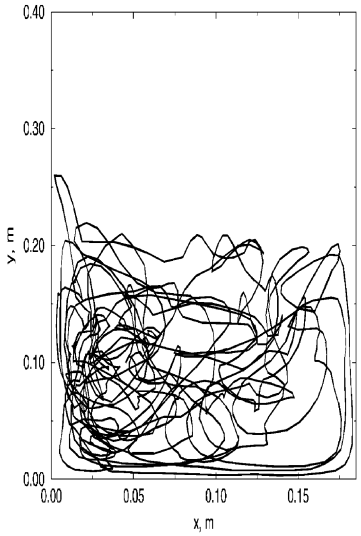

Fig. 4. Example of a trajectory of a single particle during the simulation.

From the simulation with the measured collision parameters a very similar velocity map was obtained. Although not perfectly symmetric, two circulation cells can be distinguished which is in good agreement with the PEPT data. The velocity map of the simulation assuming fully elastic, perfectly smooth collisions shows a somewhat different behaviour. The velocity vectors are smaller indicating lower speeds and also two additional circulation cells on top of the two main cells can be observed. These additional circulation cells rotate in the opposite direction and were not present in the PEPT experiment.

In Fig. 6 the occupancy plots obtained from the PEPT data and the two simulations are presented together. In this figure it can be observed that in the PEPT data the occupancy was higher near the walls which was also the case in the simulation with the measured collision parameters. This indicates that the particles spend relatively more time near the walls. In the simulation, assuming fully elastic, perfectly smooth collisions the occupancy is almost the same at each position in the system. In other words, the residence time of the particles is evenly distributed throughout the whole system. This is due to the absence of bubbles in the latter case, which causes a very homogeneous type of fluidisation.

It should be noted that the occupancy plot obtained from the PEPT data is not as smooth as the ones obtained

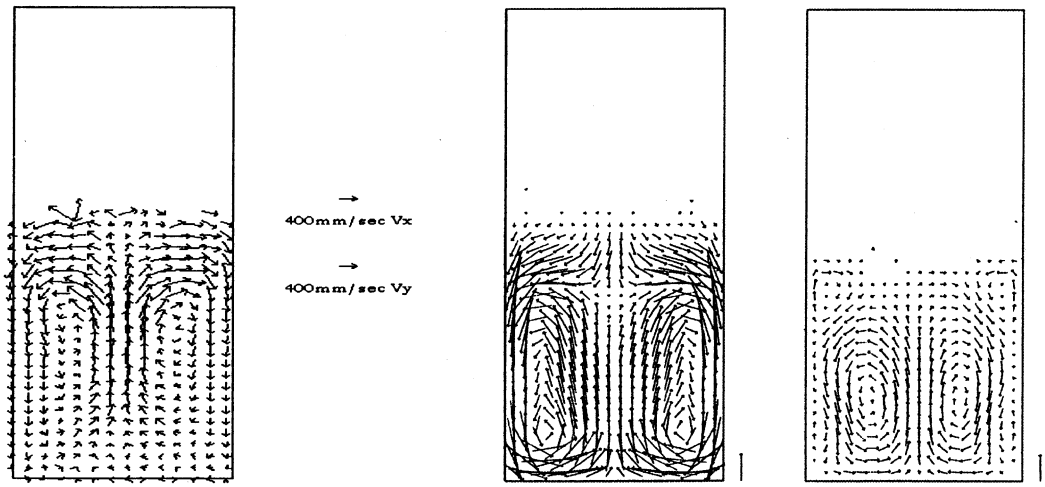

Fig. 5. Velocity map obtained from the PEPT data (left) compared with the velocity maps of the simulation using the measured collision parameters (centre) and the simulation assuming fully elastic, perfectly smooth collision (right).

from the simulations. This is obviously due to statistical limitations. For the simulation results, all the particles in the system were taken into account which renders a far smoother picture since the whole of the bed was sampled.

In Fig. 7 the speed histogram obtained from the PEPT experiment is presented together with the speed histograms obtained from the two simulations. Where the velocity map and the occupancy plot provide a basis for a more qualitative comparison between simulation and experiment, the speed histogram offers the possibility for a quantitative comparison.

In Fig. 7 it can be observed that the results of the simulation using the measured collision parameters compare rather well with the results of the PEPT experiment. Although the simulation results show a somewhat higher average speed than the PEPT data (about 0.25 m/s in the simulation and 0.15 m/s in the experiment) the shape of the distribution is rather similar. The higher average speed is most probably due to the two-dimensional nature of the simulation. The absence of the front and back walls in the simulation implies that the particles in the simulation experience a lower amount of wall friction that effectively results in a higher average speed. It is important to note that in both the experiment and the simulation particle speeds above 0.4 m/s are observed. Since these higher speeds are closely related to the bubbling behaviour in the bed, it is important that good agreement between simulation and experiment is achieved on this matter. Although the speeds observed in the simulation are somewhat higher than the ones observed in the experiment for reasons discussed above, the agreement is encouraging.

The agreement between the results of the PEPT experiment and the simulation assuming fully elastic, perfectly smooth collisions is much worse in this respect. In the latter simulation, the average speed (about 0.1 m/s) is actually closer to the average speed observed in the experi-

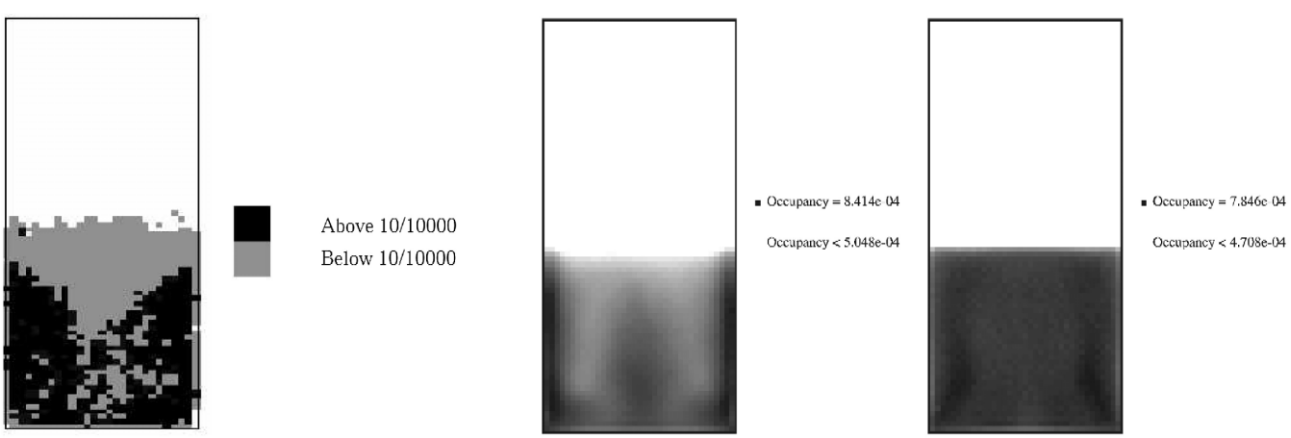

Fig. 6. Occupancy plots obtained from the PEPT data (above), the simulation using the measured collision parameters (left) and the simulation assuming fully elastic, perfectly smooth collisions (right).

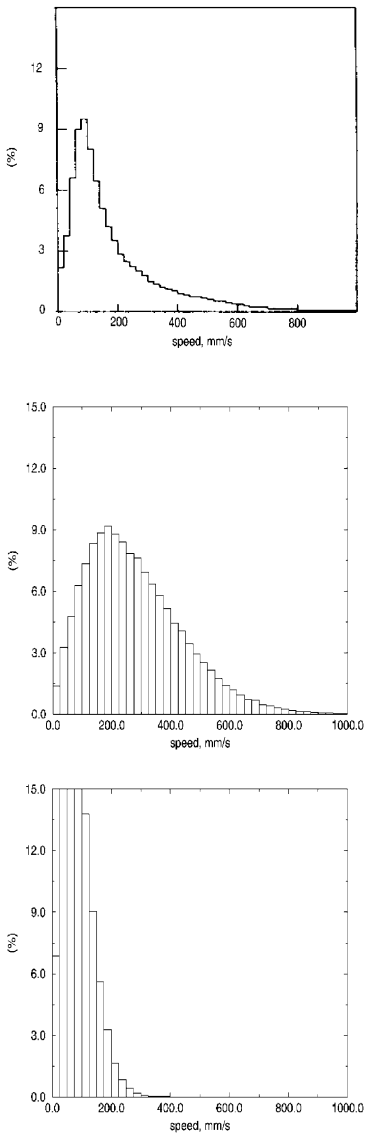

Fig. 7. Speed histogram obtained from the PEPT experiment (top) compared with the speed histograms obtained from the simulation using the measured collision parameters (middle) and the simulation assuming perfectly smooth, fully elastic collisions (bottom).

ment but more importantly however, the distribution of speeds in the histogram is far narrower: no speeds above 0.4 m/s were observed. The reason for this is the absence of bubbles in the simulation with ideal collision parameters, since the particles attain their maximum speeds when they are accelerated into the wake of a bubble. This once again emphasises the profound influence that these collision parameters have on the dynamics of a gas-fluidised bed.

6. Conclusions

Granular dynamics simulations of gas-fluidised beds with homogeneous in-flow conditions were experimentally validated using the Positron Emission Particle Tracking facility at the University of Birmingham. A quasi two-dimensional bed of 0.185-m width and 0.4 m height with homogenous inflow conditions at 1.5 u_{mf} was chosen as a test case. Glass particles ($\rho_p = 2435$ kg/m^3) with diameters ranging from 1.25 to 1.5 mm were used as the bed material. In the PEPT experiment the motion of a single tracer particle in the bed was tracked for 1 h. In the simulation, the motion of 15,000 particles was tracked for 45 s. The simulation data were time-averaged over 45 s for each particle and subsequently ensemble-averaged over all the particles in the simulation. The results showed good agreement between experiment and simulation when measured values for the collision parameters were used. The particle speeds observed in the simulation were somewhat higher than those observed in the experiment which is most probably due to the absence of the front and back wall in the simulation. When collisions were assumed to be fully elastic and perfectly smooth the agreement was worse. No speeds higher than 0.4 m/s were observed whereas in the experiment as well as in the simulation with the measured collision parameters speeds up to 0.8 m/s were found. This demonstrates the profound influence of the collision parameters on the bed hydrodynamics since these higher speeds are closely related to the presence of bubbles in the bed. From a direct comparison with an experiment, it was therefore shown that the assumption of fully elastic, perfectly smooth collisions is not valid for fluidised bed simulations.

From this first comparison between granular dynamics simulations and a PEPT experiment it can be concluded that PEPT is a powerful tool for the experimental validation of these simulations. Future work will include validation on a more detailed level (see for example Ref. [21]).

Notation

C_d	drag coefficient, [−]
e	coefficient of restitution, [−]
D_p	particle diameter, m
DT	time step, s
DX	horizontal computational cell dimension, m
DY	vertical computational cell dimension, m
g	gravitational acceleration, m/s^2
m_p	particle mass, kg
N_p	number of particles, [−]
NX	number of computational cells in x-direction, [−]
NY	number of computational cells in y-direction, [−]
p	pressure, Pa
$\boldsymbol{r}$	position vector, m
S_p	momentum source term N/m^3
T	temperature, K
t	time, s
$\boldsymbol{u}$	gas velocity vector, m/s
$\boldsymbol{v}_p$	particle velocity vector, m/s
V_p	particle volume, m^3

Greek symbols

β	volumetric interphase momentum transfer coefficient, kg/m^3 s
β_0	coefficient of tangential restitution, [−]
ε	void fraction, [−]
μ	coefficient of friction, [−]
μ_g	gas viscosity, kg/ms
τ	gas phase stress tensor, kg/ms^2
ρ	density, kg/m^3

Subscripts

c	contact point
g	gas phase
mf	minimum fluidisation
p	particle
w	wall

Acknowledgements

Aidan McCormack, Yulong Ding and Dr. David Parker of the University of Birmingham are gratefully acknowledged for their valuable contribution to the project. A.M. Kharaz en Dr. D.A. Gorham of the Open University at Milton Keynes are gratefully acknowledged for providing the collision parameters of the glass particles required for the simulations. The measurements of these collision parameters were financially supported by Unilever Research Laboratories Vlaardingen in the Netherlands.

References

[1] T.B. Anderson, R. Jackson, A fluid mechanical description of fluidized beds (equations of motion), Ind. Eng. Chem., Fundam. 6 (1967) 527.
[2] T.G. Drake, Granular flow: physical experiments and their implications for microstructural theories, J. Fluid Mech. 225 (1991) 121.
[3] S.F. Foerster, M.Y. Louge, H. Chang, K. Allia, Measurements of the collision properties of small spheres, Phys. Fluids 6 (1994) 1108.
[4] D.A. Gorham, A.H. Kharaz, Results of particle impact tests, Impact Research Group Report IRG 13, The Open University, Milton Keynes, UK, 1999.
[5] B.P.B. Hoomans, J.A.M. Kuipers, W.J. Briels, W.P.M. van Swaaij, Discrete particle simulation of bubble and slug formation in a two-dimensional gas-fluidised bed: a hard-sphere approach, Chem. Eng. Sci. 51 (1996) 99.
[6] B.P.B. Hoomans, Granular dynamics of gas–solid two-phase flows, PhD thesis University of Twente, The Netherlands, 2000.
[7] J.A.M. Kuipers, K.J. van Duin, F.P.H. van Beckum, W.P.M. van Swaaij, A numerical model of gas-fluidized beds, Chem. Eng. Sci. 47 (1992) 1913.
[8] J.A.M. Kuipers, K.J. van Duin, F.P.H. van Beckum, W.P.M. van Swaaij, Computer simulation of the hydrodynamics of a two-dimensional gas-fluidized bed, Comput. Chem. Eng. 17 (1993) 839.
[9] F. Larachi, M. Cassanello, J. Chaouki, C. Guy, Flow structure of the solids in a 3-D gas–liquid–solid fluidized bed, AIChE J. 42 (1996) 2439.
[10] J.S. Lin, M.M. Chen, B.T. Chao, A novel radioactive particle tracking facility for measurement of solids motion in gas-fluidized beds, AIChE J. 31 (1985) 465.
[11] C.C.K. Lun, Granular dynamics of slightly inelastic spheres in Couette flow, Phys. Fluids 8 (1996) 2868.
[12] T. Kawaguchi, T. Tanaka, Y. Tsuji, Numerical simulation of two-dimensional fluidized beds using the discrete element method (comparison between the two- and three-dimensional models), Powder Technol. 96 (1998) 129.
[13] T. Mikami, H. Kamiya, M. Horio, Numerical simulation of cohesive powder behavior in a fluidized bed, Chem. Eng. Sci. 53 (1998) 1927.
[14] N. Mostoufi, J. Chaouki, Prediction of effective drag coefficient in fluidized beds, Chem. Eng. Sci. 54 (1999) 851.
[15] J.J. Nieuwland, R. Meijer, J.A.M. Kuipers, W.P.M. van Swaaij, Measurements of solids concentration and axial solids velocity in gas–solid two-phase flows, Powder Technol. 87 (1996) 127.
[16] D.J. Parker, C.J. Broadbent, P. Fowles, M.R. Hawkesworth, P.A. McNeil, Positron emission particle tracking—a technique for studying flow within engineering equipment, Nucl. Instrum. Methods A 236 (1993) 592.
[17] D.J. Parker, M.R. Hawkesworth, C.J. Broadbent, P. Fowles, T.D. Fryer, P.A. McNeil, Industrial position-based imaging: principles and applications, Nucl. Instrum. Methods A 348 (1994) 583.
[18] J.F. Richardson, W.N. Zaki, Sedimentation and fluidization: part I, Trans. Inst. Chem. Eng. 32 (1954) 35.
[19] J.P.K. Seville, S.J.R. Simons, C.J. Broadbent, T.W. Martin, D.J. Parker, T.D. Beynon, Particle velocities in gas-fluidised beds, Fluid. VIII, Proc. Eng. Found. Conf. Fluid (1995) 319, Preprints Tours.
[20] M. Stein, T.W. Martin, J.P.K. Seville, P.A. McNeil, D.J. Parker, Positron emission particle tracking: particle velocities in gas-fluidised beds, mixers and other applications, in: J. Chaouki, F. Larachi, M.P. Dududkovic (Eds.), Non-invasive Monitoring of Multiphase Flows, Elsevier Science, Amsterdam, The Netherlands, 1997.
[21] M. Stein, Y.L. Ding, J.P.K. Seville, D.J. Parker, Solids motion in bubbling gas-fluidised beds, Chem. Eng. Sci. (2000) submitted for publication.
[22] C.S. Stellema, J. Vlek, R.F. Mudde, J.J.M. de Goeij, C.M. van den Bleek, Development of an improved positron emission particle tracking system, Nucl. Instrum. Methods., Phys. Res. A 404 (1998) 334.
[23] W.J. Stronge, Rigid body collisions with friction, Proc. R. Soc. Lond. A. 431 (1990) 169.
[24] M. Tan, D.J. Parker, P.R. Dee, PEPT Data Presentation Software, Manual, Birmingham University, UK, 1997.
[25] C. Thornton, Coefficient of restitution for collinear collisions of elastic-perfectly plastic spheres, J. Appl. Mech. 64 (1997) 383.
[26] Y. Tsuji, T. Kawaguchi, T. Tanaka, Discrete particle simulation of two dimensional fluidized bed, Powder Technol. 77 (1993) 79.
[27] Y. Tsuji, T. Tanaka, S. Yonemura, Cluster patterns in circulating fluidized beds predicted by numerical simulation (discrete particle model versus two-fluid model), Powder Technol. 95 (1998) 254–264.
[28] O.R. Walton, Numerical simulation of inelastic, frictional particle–particle interactions, in: M.C. Roco (Ed.), Particulate Two-Phase Flow, Part I, Butterworth-Heinemann, Boston, 1992, 884.
[29] Y. Wang, M.T. Mason, Two-dimensional rigid-body collisions with friction, J. Appl. Mech. 59 (1992) 635.
[30] J. Werther, Measurement techniques in fluidized beds, Powder Technol. 102 (1999) 15.
[31] C.Y. Wen, Y.H. Yu, Mechanics of fluidization, Chem. Eng. Prog. Symp. Ser. 62 (62) (1966) 100.
[32] B.H. Xu, A.B. Yu, Numerical simulation of the gas–solid flow in a fluidized bed by combining discrete particle method with computational fluid dynamics, Chem. Eng. Sci. 52 (1997) 2785.
[33] J.G. Yates, D.J. Cheesman, Y.A. Sergeev, Experimental observations of voidage distribution around bubbles in a fluidized bed, Chem. Eng. Sci. 49 (1994) 1885.